Chemistry–A European Journal
Research Article
doi.org/10.1002/chem.202301960
Chemistry Europe
European Chemical Societies Publishing
www.chemeurj.org

Hot Paper

Tetra-Face-Capped Octahedra in a Tetrahedra Network – Structure Determination and Scanning Transmission Electron Microscopy of $SrAl_5P_4N_{10}O_2F_3$

Monika M. Pointner,[a] Oliver Oeckler,[b] and Wolfgang Schnick*[a]

Tetrahedra-based nitridophosphates show a rich structural chemistry, which can be further extended by incorporating cations in higher coordinated positions, for example, in octahedral voids or by substituting the nitrogen atoms in the network with other anions. Following this approach, $SrAl_5P_4N_{10}O_2F_3$ was synthesized at high-temperature and high-pressure conditions using a multianvil press (1400 °C, 5 GPa) starting from $Sr(N_3)_2$, c-PON, P_3N_5, AlN, and NH_4F. $SrAl_5P_4N_{10}O_2F_3$ crystallizes in space group $I\bar{4}m2$ with $a = 11.1685(2)$ and $c = 7.84850(10)$ Å. Atomic-resolution EDX mapping with scanning transmission electron microscopy (STEM) indicates atom assignments, which are further corroborated by bond-valence sum (BVS) calculations. Ten Al^{3+}-centered octahedra form a highly condensed tetra-face-capped octahedra-based unit that is a novel structure motif in network compounds. A network of vertex-sharing PN_4 tetrahedra and chains of face-sharing Sr^{2+}-centered cuboctahedra complement the structure. Eu^{2+}-doped $SrAl_5P_4N_{10}O_2F_3$ shows blue emission ($\lambda_{em} = 469$ nm, fwhm = 98 nm; 4504 cm^{-1}) when irradiated with UV light.

Introduction

Nitridophosphates feature a large diversity of crystal structures due to the isolobal relation between P–N and Si–O bonds, which preserves a close analogy to silicate-related structural motifs like discrete tetrahedra, layers and networks.[1] Compared to silicate bonds, the elemental combination of phosphorus and nitrogen offers a more covalent bonding situation due to a smaller electronegativity difference, and thus, a more significant structural rigidity. Trivalent nitrogen substituting divalent oxygen enables motifs scarcely seen in silicates like edge-sharing tetrahedra and triply coordinated anions as well as trigonal bipyramids (PN_5), which is scarcely realized with oxygen.[2–5]

These structural modifications can result in high thermal and chemical stability and favorable mechanical, electronic, and optical properties. $MH_4P_6N_{12}$ (M = Mg, Ca), $M^{I}_3M^{III}(PO_3)_3N$ and $M^{I}_2M^{II}_2(PO_3)_3N$ (M^{I} = Li, Na; M^{III} = Al, V; M^{II} = Mg) show ion conduction, and the latter are further studied as a potential cathode material for batteries.[6–10] Eu^{2+}-doped (oxo)nitridophosphates like $AESiP_3N_7$ (AE = Sr, Ba), Ba_2PO_3N and β-$MgSrP_3N_5O_2$ are investigated as phosphor materials with intriguing luminescence properties.[11–13]

Variability in regard to structures and properties can be further increased by diversifying cations embedded in the nitridic network. Due to its capability to occupy both tetrahedra and octahedra, aluminum takes a unique role in the choice of cations concerning structural diversity. For example, in the efficient and thermally stable narrow-band emitter $Al_9O_3N_7{:}Eu^{2+}$ face- and edge-sharing $Al(O,N)_4$ tetrahedra are observed.[14] In SiAlONs, which are explored for their remarkable thermal, mechanical and chemical stability and which are employed for high-temperature engineering applications, aluminum shares tetrahedral sites with silicon and thus is part of the network.[15] Discrete $Al(O,N)_6$ octahedra are found in $Na_3Al(PO_3)_3N$, $AlP_6O_{3x}(NH)_{3-3x}N_9$ ($x \approx 0.33$), and AlP_6N_{11}.[7,16–17] Materials in the system Al/P/O/N represent catalysts with high surface areas and tuneable acid-base properties that feature excellent conversion rates and selectivity.[18–19] A more condensed structure can be found in the oxonitride Nd_2AlO_3N with vertex-sharing Al-centered octahedra.[20] Still, the pool of compounds with both a nitridophosphate network and sixfold coordinated aluminum, especially with condensed octahedra, is minimal and holds great potential for further exploration.

One area for improvement has been the availability of advanced synthesis methods. At ambient pressure, P_3N_5 decomposes above 850 °C with the formation of N_2. Therefore, high-pressure high-temperature (HP/HT) synthesis has been proposed as a viable pathway to stabilize P_3N_5 and nitridophosphates. Using stable azides and nitrides promotes the formation of N_2 and averts the decomposition of P_3N_5. This established method could be further improved by using NH_4F as a mineralizer to overcome differing reactivities of starting materials and results in new mixed nitridic networks.[11,21] Pushing for the limits of this technique and an extension of common

[a] M. M. Pointner, Prof. Dr. W. Schnick
Department of Chemistry
University of Munich (LMU)
Butenandtstraße 5–13, 81377 Munich (Germany)
E-mail: wolfgang.schnick@uni-muenchen.de
[b] Prof. Dr. O. Oeckler
Institute for Mineralogy, Crystallography and Material Science
Leipzig University
Scharnhorststraße 20, 04275 Leipzig (Germany)

Supporting information for this article is available on the WWW under https://doi.org/10.1002/chem.202301960

networks and host lattices, we work with easily accessible materials and promising elemental combinations.

Here, we report on the discovery and structural characterization of $SrAl_5P_4N_{10}O_2F_3$ containing a structural motif of ten Al^{3+}-cations in a tetra-face-capped octahedra-based topology that has not been found so far in any network compound.

Results and Discussion

Synthesis

$SrAl_5P_4N_{10}O_2F_3$ was obtained by a mineralizer-assisted high-pressure high-temperature approach at 5 GPa and 1400 °C in a multianvil press. The synthesis started from stoichiometric amounts of $Sr(N_3)_2$, cristobalite-type phosphorus oxide nitride (c-PON), P_3N_5, AlN and NH_4F as fluorine source as well as mineralizing agent (Table S1 in Supporting Information) and follows the reaction Equation (1).

$$Sr(N_3)_2 + 2\ \text{c-PON} + 2/3\ P_3N_5 + 5\ AlN + 6\ NH_4F \rightarrow SrAl_5P_4N_{10}O_2F_3 + HF + N_2 \quad (1)$$

EuF_3 was used as a doping agent to obtain Eu^{2+} luminescence. The reductive conditions upon formation of N_2 lead to the reduction of Eu^{3+}. $SrAl_5P_4N_{10}O_2F_3$ is a crystalline solid with a light-gray body color and is stable towards air and moisture. Scanning electron microscopy (SEM) images show rod-shaped crystals with a length of up to 80 μm and a width of around 30 μm (Figure S1 left). Rietveld refinement based on the PXRD data indicates no crystalline side phases (Figure 1, Table S2).

Figure S2 displays a FTIR spectrum of $SrAl_5P_4N_{10}O_2F_3$ with P–N framework vibrations between 600–1500 cm^{-1}. The weak signal around 3250 cm^{-1} corresponds to O–H vibrations, most likely due to a small extent of surface hydrolysis or a minor substitution of O^{2-} by NH^{2-}.

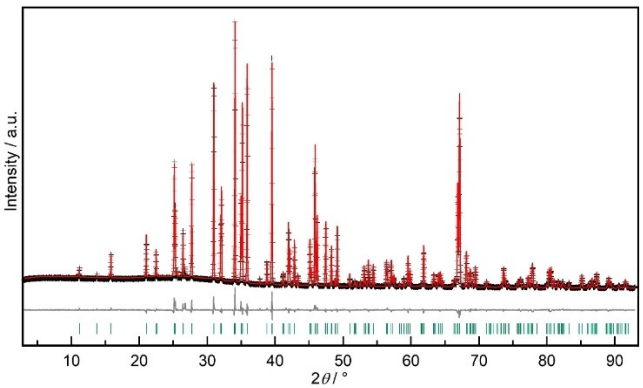

Figure 1. Rietveld refinement of $SrAl_5P_4N_{10}O_2F_3$ based on PXRD data of the bulk sample at ambient temperature with Cu–Kα_1 radiation ($\lambda = 1.5406$ Å): observed (black data points), calculated pattern (red line) and difference curve (gray line), Bragg reflection markers for $SrAl_5P_4N_{10}O_2F_3$ (green), $R_{wp} = 0.061$. No evidence for a crystalline side phase was found.

Crystal structure determination

The crystal structure of $SrAl_5P_4N_{10}O_2F_3$ was solved and refined based on single-crystal X-ray diffraction data in the tetragonal space group $I\bar{4}m2$ (no. 119, $a = 11.17931(5)$, $c = 7.85305(5)$ Å, $Z = 2$). Crystallographic data are summarized in Table 1. Wyckoff positions, atomic coordinates, and displacement parameters are given in Tables S3 and S4.

The metrics were verified by a tilt series of selected area electron diffraction (SAED) patterns and simulations based on the structure model (Figure S3). The sum formula was confirmed by TEM-EDX results taking into account BVS calculations. TEM-EDX spectroscopy data were obtained from several crystallites (example shown in Figure S1 right, results in Table S5) and agree with the expected values, particularly with respect to the atomic ratio Al : P of 1.25 : 1.

The structure contains five fully occupied cation sites and eight anion sites. The possible disorder of Al and P atoms on the octahedral and tetrahedral positions was ruled out by scanning transmission electron microscopy (STEM), including high-angle annular dark-field (HAADF) *Z*-contrast imaging and EDX mapping with atomic resolution. The corresponding intensities of the *Z*-contrast image and the spatial separation of STEM-EDX signals identify the Sr positions and confirm the allocation of Al and P on separate Wyckoff positions. The combination of the STEM-HAADF image and the corresponding STEM-EDX maps of the three cation columns Sr, Al and P along

Table 1. Crystallographic data of the single-crystal structure refinement of $SrAl_5P_4N_{10}O_2F_3$. Standard deviations are given in parentheses.

formula	$SrAl_5P_4N_{10}O_2F_3$
molar mass/g mol^{-1}	1151.00
crystal system	tetragonal
space group	$I\bar{4}m2$ (no. 119)
lattice parameters/Å	$a = 11.1685(2)$ $c = 7.84850(10)$
cell volume/Å^3	978.99(4)
formula units/unit cell	2
density/g cm^{-3}	3.905
μ/mm^{-1}	6.701
temperature/K	299(4)
absorption correction	semiempirical
Radiation	Mo-Kα ($\lambda = 0.71073$ Å)
F(000)	1104
θ range/°	3.6–36.3
total no. of reflections	15183
independent reflections [$I \geq 2\sigma(I)$ / all]	1261/1280
R_σ, R_{int}	0.0241, 0.0347
refined parameters restraints	75 0
GooF	1.073
R values [$I \geq 2\sigma(I)$]	$R1 = 0.0197$, $wR2 = 0.0438$
R values (all data)	$R1 = 0.0203$, $wR2 = 0.0441$
$\Delta\rho_{max}$, $\Delta\rho_{min}$/e Å^{-3}	1.373, −1.110

[001] are shown in Figure 2 (enlarged version Figure S4) and support the model of Al exclusively occupying octahedral sites, whereas P only occupies the single tetrahedral site. The obtained EDX spectrum is shown in Figure S5.

BVS values of all cations, all nitrogen atoms and the fluorine positions F2 and F3 agree well with the expected charges (Table 2), F1 and O1 show more significant deviations of 18% and 50%, respectively, which may imply a certain extent of O/F mixed occupation. BVS values of all nitrogen positions suggest full occupation, and the displacement parameters do not indicate partial occupancies. Minor mixed occupations in all anionic sites cannot be excluded, but data from SCXRD and BVS support the presented ordered model.

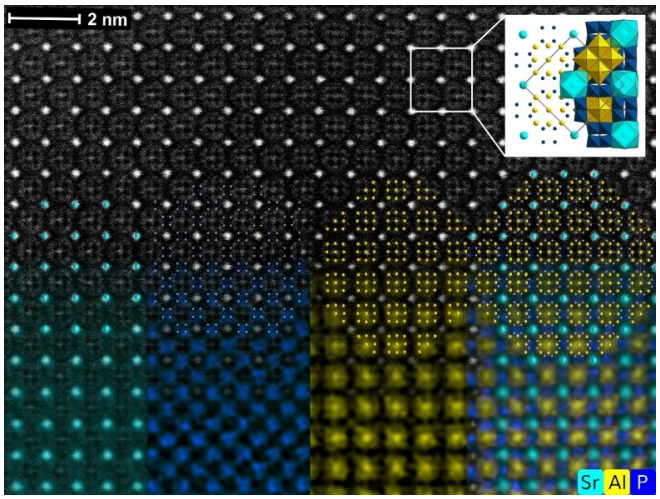

Figure 2. STEM-EDX mapping of $SrAl_5P_4N_{10}O_2F_3$ along [001]. STEM-HAADF image (top) with structure overlay (middle, Sr cyan, P blue, Al yellow). The corresponding EDX maps are shown at the bottom: Sr cyan, P blue, Al yellow, and the resulting combined map. The inset shows the unit cell.

Table 2. Calculated bond-valence sums and expected charges for the atom sites in the crystal structure of $SrAl_5P_4N_{10}O_2F_3$.

atom site	bond-valence sums	$charge_{exp.}$
Sr1	2.16	+2
P1	4.82	+5
Al1	3.20	+3
Al2	2.92	+3
Al3	2.88	+3
O1	1.47	−2
F1	1.18	−1
F2	0.92	−1
F3	0.91	−1
N1	3.13	−3
N2	2.97	−3
N3	3.01	−3
N4	2.98	−3

Structure description

The structure can be described as a distorted joint *fcc* packing of all anions and Sr atoms with partly filled octahedral and tetrahedral voids. Vertex-sharing PN_4 tetrahedra build a three-dimensional network in which Sr-centered face-sharing cuboctahedra form chains along [001]. Ten edge-sharing Al-centered octahedra build a substructure with a tetra-face-capped octahedra-based topology. An isoelectronic arrangement of the metal cations has only been observed in molecular compounds with mixed-valent $Mn^{II/III}$ ions so far.[22] Mn^{3+} ions in the cation $[Mn_{10}O_4(N_3)_4(hmp)_{12}]^{2+}$ (hmp = 2-(hydroxyl-methyl)pyridine) build an octahedron of which the non-adjacent faces are capped by four external Mn^{2+} atoms. All anions related to the complex are coordinated tetrahedrally through metal cations. In $SrAl_5P_4N_{10}O_2F_3$ the same tetra-face-capped octahedra-based topology is formed by cations and all cationic positions are occupied by Al^{3+}. Anionic positions differ slightly from the literature. Two anionic positions are coordinated tetrahedrally and one position occupies an octahedral coordination. This is the first case of a network compound in which such a structure motif occurs. For better visualization, the unit cell in Figure 3 shows only one Al_{10} unit (yellow), one chain of Sr-centered cuboctahedra (cyan) and the PN_4 tetrahedra network (dark blue). Figure 4 illustrates all coordination polyhedra.

Vertex-sharing PN_4 tetrahedra form corrugated ten- and eight-membered rings (Figure S6). P–N distances and N–P–N angles vary between 1.6141(18)–1.6708(15) Å and 105.33(12)–122.44(8)°, respectively, which is in good agreement with known nitridophosphates.[23–25]

The strontium atoms occupy a single crystallographic site, which is coordinated by N, O and F atoms, leading to a $Sr(N_6O_2F_4)$ cuboctahedra. The Sr atom position is somehow modulated along [100], resulting in shorter (3.4799(10) Å) and longer (4.3686(10) Å) $d_{Sr\text{-}Sr}$ that deviate by ≈11% from an average value of 3.9242 Å. This leads to more acute Sr–N–Sr angles of 76.94(5)° between the shorter Sr–Sr distances compared to the more obtuse Sr–F–Sr angles of 102.82(5)° associated with the larger Sr–Sr distances (Figure S7). Even with this alternation of the Sr–Sr chain, interatomic distances within the cuboctahedra reveal only a small overall distortion of the single cuboctahedron.

The topology of the cations in the Al_{10} unit has been described as a tetra-face-capped octahedron.[22] In literature,

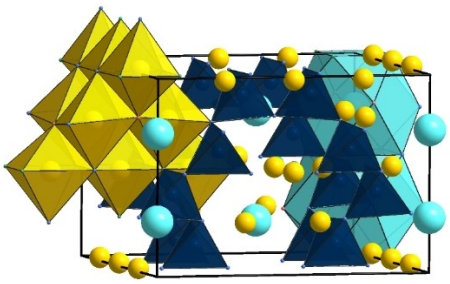

Figure 3. Illustration of a $SrAl_5P_4N_{10}O_2F_3$ unit cell with $Sr(N_6O_2F_4)$ cuboctahedra (cyan), one $(Al(N,O,F)_6)_{10}$ unit (yellow) and PN_4 tetrahedra (dark blue).

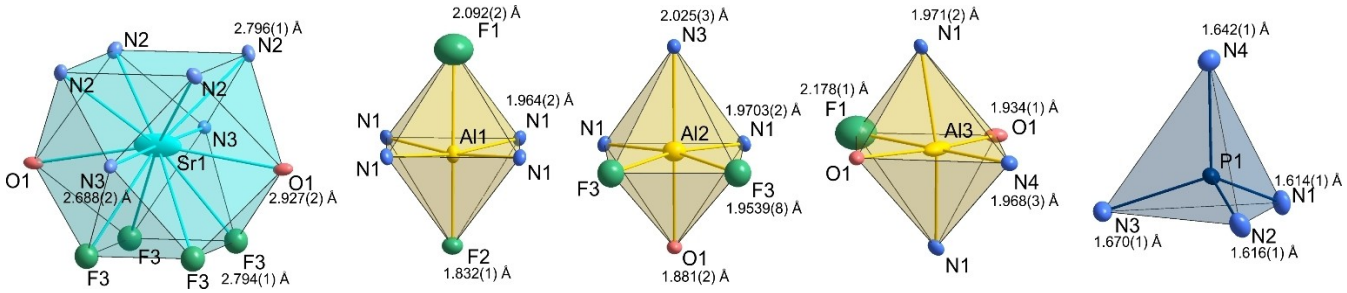

Figure 4. Coordination polyhedra around Sr1, Al1, Al2, Al3 and P1. Displacement ellipsoids are shown for 90 % probability.

anions are surrounded by four metal cations, forming tetrahedra. Here, the central anion F1 is surrounded by six Al^{3+} ions (Al1 + Al3), forming an octahedron. All twelve edges are bridged by eight nitrogen atoms and four oxygen atoms (Figure 5). All bridging anions are linked to external Al^{3+} ions (Al2). The units are connected to each other through vertices. Al2- and Al1-centered octahedra share common F3 and F1 atoms, respectively (Figure 6a)). Al_{10} units alternate with the Sr-centered cuboctahedra chains along the directions *a* and *b* (Figure 6b)).

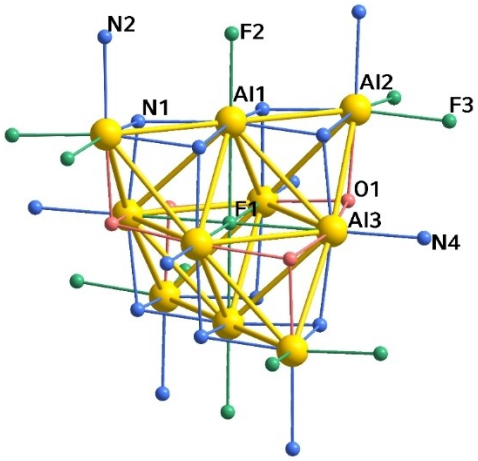

Figure 5. Partially labeled representation of an Al_{10} unit with Al^{3+} yellow, O light red, N light blue, F light green and bonds from Al^{3+} ions to Al^{3+} anions in respective colors. Ten Al^{3+} cations build a tetra-capped octahedron, marked with yellow lines between Al^{3+} ions. The central octahedron is occupied by F1.

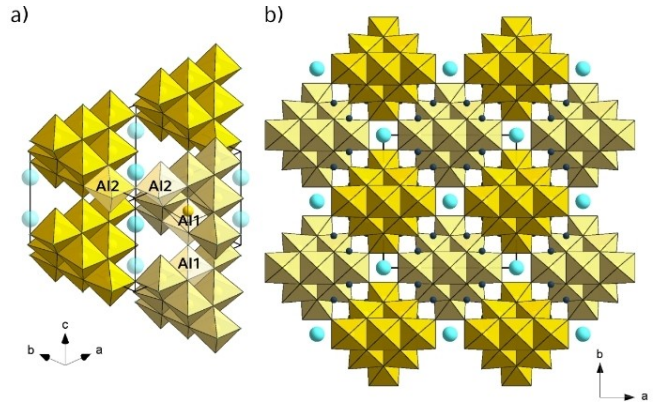

Figure 6. Illustration of the Al_{10} substructure. Light and dark yellow for better distinction; a) Octahedra sharing vertices are partially highlighted: Common F3 anions connect Al2 octahedra in the [001] plane, common F1 atoms connect Al1 octahedra along the *c* axis b) Alternating Al_{10} units and Sr columns in [001]. Sr cyan, $(Al(N,O,F)_6)_{10}$ units (yellow, light yellow), P (dark blue).

The three crystallographically independent Al^{3+} ions differ in their coordinating anions leading to AlN_4F_2, AlN_3OF_2 and AlN_3O_2F octahedra. They are slightly distorted and tilted against each other, with the Al^{3+} atoms slightly displaced from the centers. The distances of the aluminum atoms to their neighboring anions vary between 1.8319(14)–2.1778(10) Å and increase from Al–O (1.916 Å) to Al–N (1.973 Å), as expected. However, Al–F bond lengths do not follow the trend with the shortest and longest average distance found for Al–F bonds. Some Al–F bonds are unexpectedly long, for example, Al1-F1/ Al3-F1 with 2.0924(14)/ 2.1778(10) Å. An overview of interatomic distances and angles is provided in Table S6 and S7.

Luminescence

To investigate luminescence properties, Eu^{2+}-doped samples have been synthesized by adding ≈1 mol % of EuF_3, referring to the Sr content to the starting mixtures. EuF_3 was chosen as a europium source to support the formation of HF additionally. The photoluminescence properties were investigated on single particles (Figure S8). The blue luminescence of $SrAl_5P_4N_{10}O_2F_3$ most likely originates from Eu^{2+} located on a cuboctahedrally coordinated Sr^{2+} site, owing to similar ionic radii of Eu^{2+} and Sr^{2+}. In addition, the highly condensed PN_4 network with additional $Al(N,O,F)_6$ octahedra leaves no other suitable position for a possible luminescence center with respect to the ion sizes.

The Eu^{2+}-doped material features a strong blue emission with a single broad emission maximum peaking at λ_{em} = 469 nm upon excitation with λ_{exc} = 390 nm. The full width at half maximum is 98 nm (4504 cm^{-1}). Emission from Eu^{2+} on a highly symmetric site often results in a narrow emission band, as observed in AEP_8N_{14} (*AE* = Ca, Sr) or $AEBe_{20}N_{14}$:Eu^{2+} (*AE* = Sr, Ba).[25–26] $SrAl_5P_4N_{10}O_2F_3$ provides a symmetric, only slightly distorted cuboctahedral coordination around the alkaline earth atom. The relatively broad emission band probably results from the displacement of the Sr atom out of the center of the cuboctahedron. Furthermore, the three different anions N, O

and F surrounding Eu^{2+} generate an inhomogeneous ligand field, which further broadens the emission band.

Nitrides tend to have a red-shifted emission compared to oxonitrides because *AE*-N bonds are more covalent than *AE*-O/-F bonds. In the case of $SrAl_5P_4N_{10}O_2F_3$:Eu^{2+}, the position of the emission maximum is thus rather comparable to oxides and oxonitrides like $SrLi_2Be_4O_6$:Eu^{2+} or $Sr_{0.25}Ba_{0.75}Si_2O_2N_2$:$Eu^{2+}$ (CN = 8, λ_{em} = 456 and 472 nm,) than to nitrides such as Sr[$LiAl_3N_4$]:Eu^{2+} (λ_{em} = 650 nm).[27–29]

Conclusions

An NH_4F-mediated HP/HT synthesis obtained $SrAl_5P_4N_{10}O_2F_3$. Its successful synthesis with a mineralizer-assisted approach demonstrates the feasibility to employ different potentially inert starting materials to form mixed nitride networks.[11] The crystal structure was determined by single-crystal X-ray diffraction and is consistent with element ratios from EDX. STEM-EDX mapping with atomic resolution and high-angle annular dark-field *Z*-contrast images confirm the cation site assignment. The crystal structure can be described as a network of vertex-sharing PN_4 tetrahedra, chains of face-sharing Sr-centered cuboctahedra and a substructure of condensed Al_{10} units formed by ten edge-sharing $Al(N,O,F)_6$ octahedra, yet unseen in network structures.

$SrAl_5P_4N_{10}O_2F_3$ is suitable as a host lattice for rare-earth activator ions and shows blue emission upon doping with Eu^{2+}. This highlights the potential for the development of new host compounds for phosphors with mixed alkaline earth and aluminum cations. In theory, a large number of charge-balanced compounds with diverse structural motifs can be accessed. A possible site-selectivity of doping due to differences in ionic radii of Al^{3+} and AE^{2+} and charges (e.g., Ce^{3+} on Al^{3+} sites versus Eu^{2+} on AE^{2+} sites) makes the research on aluminum-containing nitrides and nitridophosphates a promising field worth investigating.

Experimental Section

Preparation of starting materials: P_3N_5 was prepared by heating P_4S_{10} (Sigma-Aldrich, 99.99%) in a constant ammonia flow.[30] After drying (at 1273 K) a fused silica tube and silica boat under dynamic vacuum ($< 10^{-3}$ bar), P_4S_{10} was loaded into the boat in a constant flow of argon. The setup was purged with dry ammonia (Air Liquide, 5.0) for 4 h, and the reaction was carried out at 1123 K for 4 h. The furnace was cooled to room temperature (heating and cooling ramp of 5 K/min), and the product was washed with diluted HCl and H_2O. The product was obtained as an orange powder. PXRD and CHNS analyses confirmed its purity (in wt%: C 0%, H 0%, N 42.69%, S 0%; expected C 0%, H 0%, N 42.98%, S 0%). PON was synthesized according to the literature, and PXRD confirmed the phase purity.[31]

Multianvil synthesis: $SrAl_5P_4N_{10}O_2F_3$ was synthesized under high-pressure high-temperature conditions (T = 1400 °C, p = 5 GPa) using a 1000 t hydraulic press (Voggenreiter, Mainleus, Germany) with a modified Walker module. Details on the preparation and handling of the 1000 t Walker-type multianvil press are described in the literature.[32–35] Stoichiometric amounts of the starting materials $Sr(N_3)_2$, AlN, PON, P_3N_5 and 3 wt.% NH_4F (Table S1) were thoroughly mixed in an agate mortar in an Ar-filled glovebox (Unilab, MBraun, Garching, $O_2 < 1$ ppm, $H_2O < 0.1$ ppm), transferred into a crucible of h-BN (HeBoSint® S100, Henze, Kempten, Germany) and sealed with a h-BN lid. After sample insertion, the setup was compressed to 5 GPa and heated to 1400 °C within 60 min. The temperature was kept constant for 300 min before cooling to room temperature and slowly decompressing.

Powder X-ray diffraction (PXRD): A powder diffractometer Stadi P (Stoe & Cie GmbH, Darmstadt, Germany) with Cu–Kα_1 radiation (λ = 1.54056 Å; Ge(111) single-crystal monochromator) with parafocusing Debye–Scherrer geometry and MYTHEN 1 K Si strip detector (Dectris Ltd., Baden, Switzerland) was used. Powder diffractograms of finely ground samples in glass capillaries (Ø 0.3 mm, wall thickness 0.01 mm, Hilgenberg GmbH, Malsfeld, Germany) were recorded at an angular range of 2θ = 3–93°. TOPAS Academic 6.1 was used for Rietveld refinements, employing a fundamental parameters approach and a Chebyshev polynomial for background modelling.[36–37]

Energy-dispersive X-ray spectroscopy (EDX): Isolated crystals of the sample were placed on a conducting carbon foil and coated with carbon. A FEI Gelios Nanolab G3 Dual Beam UC (Fei, Hillsboro, OR, USA) with an attached X-Max 80 SDD detector (Oxford Instruments, Abingdon, UK) obtained EDX spectra.

Scanning transmission electron microscopy (STEM): The sample was ground thoroughly in absolute ethanol and distributed on a lacey carbon film covered Cu grid (S-166-2, Plano GmbH, Lünen, Germany) and mounted in a double-tilt holder (±30°). STEM was carried out with a Titan Themis 300 (FEI, USA) transmission electron microscope equipped with an X-FEG source, a post-column filter (Enfinium ER-799), a Cs DCOR probe corrector, a US1000XP/FT camera system (Gatan, Germany), a 4k×4k FEI Ceta CMOS camera (FEI, USA) and a windowless 4-quadrant Super-X EDX detector. The system was operated at an acceleration voltage of 300 kV. Data processing was performed with the following software: Digital Micrograph (Fourier filtering of STEM images), ProcessDiffraction7 (calculations of SAED patterns), JEMS (SAED simulations) and Velox (STEM images, EDX maps).[38–41]

Single-crystal X-ray diffraction (SCXRD): A Bruker D8 Venture TXS diffractometer (rotating anode, Mo–Kα radiation, λ = 0.71073 Å, multilayer monochromator) was used to obtain single-crystal X-ray diffraction data. For indexing, integration and semiempirical absorption correction, the program package APEX3 was used.[42–43] Structure solution was performed with direct methods (SHELXS), whereas the structure refinement was conducted using the full-matrix least-squares methods (SHELXL-2018).[44] For visualization, Diamond3 was used.[45] VaList was used to perform BVS calculations.[46–47]

Deposition Number(s) 2261405 contain(s) the supplementary crystallographic data for this paper. These data are provided free of charge by the joint Cambridge Crystallographic Data Centre and Fachinformationszentrum Karlsruhe Access Structures service.

FTIR spectroscopy: An FTIR spectrum was recorded on a Spectrum BX II spectrometer (PerkinElmer Waltham, MA, USA) with a DuraSampler ATR unit in the range of 650–4400 cm^{-1}.

Luminescence measurements: Luminescence measurements of single crystals of $SrAl_5P_4N_{10}O_2F_3$:Eu^{2+} were carried out on small particles in air. The spectrum was obtained on a HORIBA Fluoromax4 spectrofluorimeter system with an Olympus BX51 microscope. Emission spectra of the single crystals ranged from 400 to 800 nm (step size of 2 nm) and were collected at room temperature after excitation with blue light (λ_{exc} = 390 nm).

Acknowledgements

Financial support by the Deutsche Forschungsgemeinschaft DFG (projects SCHN 377/18-1 and OE 513/6-1) is gratefully acknowledged. The authors thank Dr. Peter Mayer and Christian Minke for single-crystal data collection and SEM measurements, respectively (all at LMU Munich) and Dr. Philipp Strobel (Lumileds Phosphor Center Aachen) for luminescence measurements. Open Access funding enabled and organized by Projekt DEAL.

Conflict of Interests

The authors declare no conflict of interest.

Data Availability Statement

The data that support the findings of this study are available in the supplementary material of this article.

Keywords: Aluminum · anionic framework · electron microscopy · high-pressure chemistry · solid-state structures

[1] S. D. Kloß, W. Schnick, *Angew. Chem.* **2019**, *131*, 8015–8027; *Angew. Chem. Int. Ed.* **2019**, *58*, 7933–7944.
[2] D. Baumann, W. Schnick, *Angew. Chem.* **2014**, *126*, 14718–14721; *Angew. Chem. Int. Ed.* **2014**, *53*, 14490–14493.
[3] S. Horstmann, E. Irran, W. Schnick, *Z. Anorg. Allg. Chem.* **1998**, *624*, 221–227.
[4] W. Schnick, *Angew. Chem.* **1993**, *105*, 846–858; *Angew. Chem. Int. Ed. Engl.* **1993**, *32*, 806–818.
[5] D. Baumann, W. Schnick, *Inorg. Chem.* **2014**, *53*, 7977–7982.
[6] A. Marchuk, V. R. Celinski, J. Schmedt auf der Günne, W. Schnick, *Chem. Eur. J.* **2015**, *21*, 5836–5842.
[7] K. Higashi, M. Ochi, Y. Nambu, T. Yamamoto, Taito Murakami, N. Yamashina, C. Tassel, Y. Matsumoto, H. Takatsu, C. M. Brown, H. Kageyama, *Inorg. Chem.* **2021**, *60*, 11957–11963.
[8] M. R. Cosby, G. S. Mattei, Y. Wang, Z. Li, N. Bechtold, K. W. Chapman, P. G. Khalifah, *J. Phys. Chem. C* **2020**, *124*, 6522–6527.
[9] J. Liu, X. Yu, E. Hu, K.-W. Nam, X.-Q. Yang, P. G. Khalifah, *Chem. Mater.* **2013**, *25*, 3929–3931.
[10] M. Reynaud, A. Wizner, N. A. Katcho, L. C. Loaiza, M. Galceran, J. Carrasco, T. Rojo, M. Armand, M. Casas-Cabanas, *Electrochem. Commun.* **2017**, *84*, 14–18.
[11] L. Eisenburger, O. Oeckler, W. Schnick, *Chem. Eur. J.* **2021**, *27*, 4461–4465.
[12] S. Wendl, M. Mallmann, P. Strobel, P. J. Schmidt, W. Schnick, *Eur. J. Inorg. Chem.* **2020**, *10*, 841–846.
[13] R. M. Pritzl, N. Prinz, P. Strobel, P. J. Schmidt, D. Johrendt, W. Schnick, *Chem. Eur. J.* **2023**, e202301218.
[14] J. Ding, Y. Wei, W. Liu, Y. Li, Q. Wu, J. Zhou, *Chem. Eng. J.* **2021**, *403*, 126382.
[15] K. H. Jack, W. I. Wilson, *Nat. Phys. Sci.* **1972**, *238*, 28–29.
[16] L. Neudert, F. Heinke, T. Bräuniger, F. J. Pucher, G. B. Vaughan, O. Oeckler, W. Schnick, *Chem. Commun.* **2017**, *53*, 2709–2712.
[17] S. J. Ambach, M. Pointner, S. Falkai, C. Paulmann, O. Oeckler, W. Schnick, *Angew. Chem.* **2023**, e202303580; *Angew. Chem. Int. Ed.* **2023**, e202303580.
[18] P. Grange, P. Bastians, R. Conanec, R. Marchand, Y. Laurent, L. Gandia, M. Montes, J. Fernandez, J. A. Odriozola in *Studies in Surface Science and Catalysis*, Elsevier, **1995**, *91*, pp. 381–389.
[19] E. Guéguen, S. Delsarte, V. Peltier, R. Conanec, R. Marchand, Y. Laurent, P. Grange, *J. Eur. Ceram. Soc.* **1997**, *17*, 2007–2010.
[20] R. Marchand, *Rev. Chim. Miner.* **1982**, *19*, 684–689.
[21] L. Eisenburger, V. Weippert, O. Oeckler, W. Schnick, *Chem. Eur. J.* **2021**, *27*, 14184–14188.
[22] T. C. Stamatatos, K. A. Abboud, W. Wernsdorfer, G. Christou, *Angew. Chem.* **2006**, *118*, 4240–4243; *Angew. Chem. Int. Ed.* **2006**, *45*, 4134–4137.
[23] F. J. Pucher, A. Marchuk, P. J. Schmidt, D. Wiechert, W. Schnick, *Chem. Eur. J.* **2015**, *21*, 6443–6448.
[24] A. Marchuk, S. Wendl, N. Imamovic, F. Tambornino, D. Wiechert, P. J. Schmidt, W. Schnick, *Chem. Mater.* **2015**, *27*, 6432–6441.
[25] S. Wendl, L. Eisenburger, P. Strobel, D. Günther, J. P. Wright, P. J. Schmidt, O. Oeckler, W. Schnick, *Chem. Eur. J.* **2020**, *26*, 7292–7298.
[26] E. Elzer, R. Niklaus, P. J. Strobel, V. Weiler, P. J. Schmidt, W. Schnick, *Chem. Mater.* **2019**, *31*, 3174–3182.
[27] P. Strobel, C. Maak, V. Weiler, P. J. Schmidt, W. Schnick, *Angew. Chem.* **2018**, *57*, 8875–8879; *Angew. Chem. Int. Ed.* **2018**, *57*, 8739–8743.
[28] M. Seibald, T. Rosenthal, O. Oeckler, F. Fahrnbauer, A. Tücks, P. J. Schmidt, W. Schnick, *Chem. Eur. J.* **2012**, *18*, 13446–13452.
[29] P. Pust, V. Weiler, C. Hecht, A. Tücks, A. S. Wochnik, A.-K. Henß, D. Wiechert, C. Scheu, P. J. Schmidt, W. Schnick, *Nat. Mater.* **2014**, *13*, 891–896.
[30] A. Stock, H. Grüneberg, *Ber. Dtsch. Chem. Ges.* **1907**, *40*, 2573–2578.
[31] S. Vogel, D. Baumann, R. Niklaus, E. Bykova, M. Bykov, N. Dubrovinskaia, L. Dubrovinsky, W. Schnick, *Angew. Chem.* **2018**, *130*, 6801–6805; *Angew. Chem. Int. Ed.* **2018**, *57*, 6691–6695.
[32] D. Rubie, *Phase Transitions* **1999**, *68*, 431–451.
[33] H. Huppertz, *Z. Kristallogr.* **2004**, *219*, 330–338.
[34] D. Walker, *Am. Mineral.* **1991**, *76*, 1092–1100.
[35] D. Walker, M. Carpenter, C. Hitch, *Am. Mineral.* **1990**, *75*, 1020–1028.
[36] A. Coelho, *Coelho Software*, Version 6.1, Brisbane (Australia), **2007**.
[37] H. M. Rietveld, *J. Appl. Crystallogr.* **1969**, *2*, 65–71.
[38] I. Gatan, *DigitalMicrograph*, Version 3.6.5, Pleasanton, California (USA), **1999**.
[39] J. L. Lábár, *Ultramicroscopy* **2005**, *103*, 237–249.
[40] J. P. Stadelmann, jEMS software package, Version 3.60907U2011, Saas-Fee (Switzerland), **1999–2011**.
[41] Thermo Fisher Scientific, *Velox*, Waltham, Massachusetts (USA), **2021**.
[42] Bruker-AXS, *APEX3*, Version 2016.5-0, Karlsruhe (Germany), **2001**.
[43] G. M. Sheldrick, *Acta Crystallogr. Sect. A* **2008**, *71*, 112–122.
[44] G. M. Sheldrick, *Acta Crystallogr. Sect. C* **2015**, *71*, 3–8.
[45] K. Brandenburg, *Diamond*, Version 3.2k, Bonn (Germany), 1997–2014.
[46] A. S. Wills, *VaList – A bond valence calculation and analysis program*, Version 4.0.7, University College London, London (UK), 1998–2010.
[47] N. E. Brese, M. O'Keeffe, *Acta Crystallogr. Sect. B* **1991**, *47*, 192–197.

Manuscript received: June 20, 2023
Accepted manuscript online: July 6, 2023
Version of record online: August 17, 2023